JOURNAL OF PROPULSION AND POWER
Vol. 24, No. 1, January–February 2008

Magnetic Sensing of Azimuthal Current in Hall Thrusters: In-Flight Diagnostic Potential

Binyamin Rubin,* Alexander Kapulkin,† and Moshe Guelman‡
Technion–Israel Institute of Technology, 32000 Haifa, Israel

DOI: 10.2514/1.24572

In this paper, the method of Hall current spatial structure estimation based on the measurements of steady-state magnetic fields induced by this current outside the acceleration channel is proposed. The approach to Hall current structure determination is based on the inverse magnetostatic problem solution using two-dimensional constrained regularization. The optimal number and positions of magnetic sensors are determined, and the solutions using simulated measurements with and without simulated noise are obtained.

Nomenclature

A	=	kernel matrix
a, b, c	=	numerical parameters
B	=	magnetic flux density
B_r	=	magnetic flux density radial component
B^*	=	magnetic flux density radial component with added simulated noise
D	=	relative error in the regularized solutions
d	=	error level in simulated measurements
E	=	electric field
E_z	=	electric field axial component
e	=	unit positive electric charge
I_H	=	normalization coefficient
I_{tot}	=	total Hall current value
j_H	=	Hall current density
j_{iq}	=	ion current density
j^{exact}	=	Hall current density exact distribution
j^{inverse}	=	Hall current density distribution obtained from the inverse problem solution
L	=	regularization matrix
M	=	mass of ion
m	=	mass of electron
n	=	electron (ion) number density
r	=	radial coordinate
S	=	acceleration channel cross section
T	=	thrust
V	=	ion velocity
z	=	axial coordinate
ε	=	ion energy
λ	=	regularization parameter
ξ	=	normally distributed random number
σ_0	=	electric conductivity
τ_e	=	time between collisions of the electron with heavy particles or walls
Φ	=	electric potential
ω_e	=	electron cyclotron frequency
$\omega_e\tau_e$	=	Hall parameter

Received 11 April 2006; revision received 1 March 2007; accepted for publication 10 July 2007.

*Ph.D. Student, Faculty of Aerospace Engineering; currently Postdoctoral Researcher, Electric Propulsion and Plasma Engineering Laboratory, Department of Mechanical Engineering, Colorado State University; brubin@engr.colostate.edu.

†Senior Scientist, Asher Space Research Institute.

‡Asher Space Research Institute; currently Institute Director and Professor, Faculty of Aerospace Engineering.

I. Introduction

MODERN electric propulsion systems and in particular, Hall thrusters, are often equipped with diagnostic packages. The main purpose of these packages is usually to investigate the thruster performance as well as the environment created during the electric propulsion system's operation and its influence on the spacecraft. The diagnostics of the internal thruster processes are also of great interest. The results of onboard measurements show that the operation of a Hall thruster in space may differ from its operation during ground tests [1,2]. To understand the reasons for these differences, a study of processes in the thruster acceleration channel should be done during flight. Another important reason for the creation of an onboard diagnostics system is that it may provide clues to understanding the possible thruster malfunctions. The obvious requirements to such systems are compactness, a light weight, and the capability of noncontact real-time measurements without affecting thruster operation. In previous works [3,4] different types of onboard diagnostics systems capable of providing information on the internal processes in the Hall thruster were proposed. This paper is devoted to the method of noncontact determination of the Hall current structure using magnetic field sensors.

The structure of the Hall current was previously investigated using probe measurements [5–7] as well as a noninvasive method, which requires the thruster to be switched off during each measurement's run [8–11]. The approach described in the present work allows carrying out steady-state measurements, which is especially important for onboard systems. The method is based on noncontact measurements of the steady-state magnetic field induced by the Hall current outside the acceleration channel. The approach to the Hall current structure determination is based on the inverse magnetostatic problem solution using a two-dimensional constrained regularization. Optimal number and positions of magnetic sensors are determined, and the solutions using simulated measurements with and without simulated noise are obtained.

The study of the Hall current distribution is of interest for several reasons. The magnetic field in the Hall thruster is the sum of both the applied and the self-magnetic fields. The self-magnetic field is mainly due to the Hall current. Therefore, to determine the magnetic field configuration, it is necessary to know the Hall current's distribution. This is especially important for high-power Hall thrusters because the Hall current and consequently the self-magnetic field grows with the thruster's power level increase. Furthermore, knowledge of the electric field distribution and ion flow parameters inside the acceleration channel is of prime importance for the Hall thruster's design. These distributions could be obtained using diagnostic probes in the acceleration channel. However, for thrusters, having sizes and current densities typical of flight models, the damage caused to the diagnostic probes by the flow of the fast ions, as well as the probe's influence on the thruster discharge, make their use problematic. These distributions may be obtained under laboratory conditions, without introducing diagnostic sensors into

the acceleration channel, by using a set of magnetic sensors as presented in this paper in combination with a retarding potential analyzer and collector of ions placed beyond the thruster.

II. Direct Problem

A. Method of Solution

The direct problem is the calculation of the magnetic field (self-field) generated by the Hall current. The magnetic field distribution in the Hall thruster is not exactly axially symmetric because of the outer magnetic coils. In most cases, the deviation of the magnetic field distribution from axially symmetric may be neglected, but in our case, it should be taken into account to measure the small field generated by the Hall current. Furthermore, the outer magnetic screen is not axisymmetric because of the required modifications to allow placement of magnetic sensors in the vicinity of the Hall thruster. Consequently, it is impossible to use a simplified two-dimensional axisymmetric model, and fully 3-D calculations are necessary. The calculations were performed using the ANSYS finite-element method (FEM) solver.

The magnetic circuit of the Hall thruster includes the following parts: inner and outer magnetic coils with magnetic cores, inner and outer magnetic pole pieces, inner and outer magnetic screens, and the backplane. The coils generate the magnetic field in the magnetic cores. This field is directed through the pole pieces into the acceleration channel region adjacent to the thruster exit plane. The magnetic flux lines going from the inner to the outer pole pieces create a so-called magnetic lens in the acceleration channel. The backplane provides the path to close the magnetic field lines in the back part of the thruster. The magnetic screens reduce the magnetic field in the inner part of the acceleration channel. It is necessary to reduce the electric field in the inner part of the channel and to increase the electric field in the near-exit region where the ion acceleration occurs.

The model of the magnetic system typical of present-day low-power Hall thrusters was chosen for calculations (Fig. 1). The length of the magnetic system is 48 mm, the diameter (outer) of the inner magnetic screen is 31 mm, and the diameter (inner) of the outer magnetic screen is 77 mm. The cylindrical outer magnetic screen was modified near the thruster exit plane as shown in Fig. 1: four rectangular boxes were cut into the screen equally spaced in the azimuthal direction. The dimensions of the box are 17 mm in the axial direction, 12 mm in the azimuthal direction, and 8.5 mm in the radial direction. The modification allows placing the magnetic sensors (for example, commercial Honeywell HTMC1021D) in the vicinity of the Hall current.

The mass of the Hall thruster before modification is about 2 kg. The overall mass increase due to the modification of the magnetic screen and installation of both the measurement system and telemetry is expected to be below 0.3 kg.

The model of the Hall thruster used in the calculations has moderate size and power. Application of the proposed technique for larger, more powerful thrusters would be simpler. The level of the primary magnetic field in larger thrusters is approximately the same as in small ones, whereas the Hall current and its self-magnetic field increase with the increase in thruster size and power. Therefore, the ratio of the Hall current's self-magnetic field to the primary magnetic field increases. It is desirable to use the proposed measurements technique because it will increase the measurement accuracy. Additionally, in larger thrusters there is more space available for sensor placement.

Because a broad range of oscillations occurs in the Hall thruster plasma, filtering and averaging of the measured magnetic field values are necessary to calculate average Hall current distribution.

The Hall current distribution was approximated by cylindrical current elements. We determined that a size of 1.4×1.5 mm for each element gives sufficiently accurate results at reasonable computational time; the total number of elements was 130. It should be noted that although the problem is three-dimensional, the current distribution is axisymmetric and therefore is treated as two dimensional.

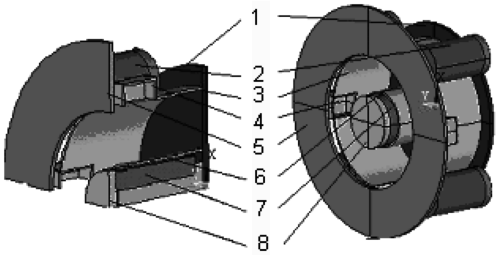

Fig. 1 Full and quarter sector model geometry of modified magnetic system. 1) Backplane; 2) outer magnetic coil; 3) outer magnetic screen; 4) modified part of the magnetic screen; 5) outer magnetic pole piece; 6) inner magnetic screen; 7) inner magnetic coil; 8) inner magnetic pole piece.

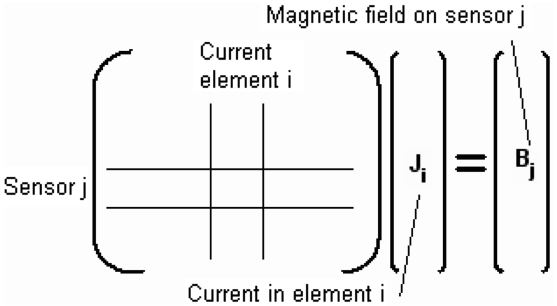

Fig. 2 Linear system used for magnetic field calculation.

The solution of the inverse problem is an iterative process that includes one or more calculations of the direct problem solution at every iteration. It is possible to use an FEM solver in these calculations, but the computational time in this case will be unreasonably high. Because the dependence between the current and the magnetic flux density may be considered as linear in the range of magnetic field values generated by the Hall current, the distribution of the magnetic field may be obtained as the linear combination of the magnetic fields of individual elements. Calculating the magnetic field distribution generated by each of the N current elements placing M magnetic field sensors, each measuring one magnetic field component, we obtain the linear matrix equation shown in Fig. 2.

The elements of this matrix are the values of the magnetic field at different sensor locations generated by the current element carrying unit current. To calculate the magnetic field generated by a specific current distribution, this matrix is multiplied by the column-wise stacked vector of current distribution.

The obtained matrix may be easily checked experimentally using the method described in [8–11]. A metal coil carrying current should be placed into the acceleration channel, and the magnetic field generated by the coil should be measured for different coil locations.

B. Results of Direct Problem Solution

The radial magnetic field profile for the original and modified magnetic systems is presented in Fig. 3. The profiles closely match; the maximum difference of the centerline values is about 5%. The maximum variation of the magnetic field on the outer wall of the acceleration channel is about 10%.

According to the different experimental data available up to date [5–11], the Hall current is 3.5–15 times higher then the discharge current. For the Hall thruster model with dimensions used in our analysis, the discharge current value is about 2A; therefore, the Hall current value of 10A was chosen as a conservative estimation, which corresponds to typical values of the effective Hall parameter in the range of 200–300 [12].

For the purpose of simulating the magnetic field measurements, the following decomposition of the Hall current density distribution was used:

$$j_H = I_H Z(z) R(r)$$

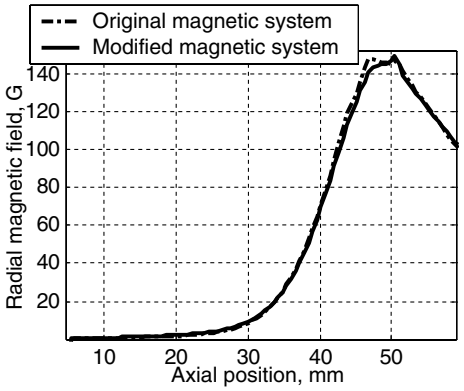

Fig. 3 Comparison of radial magnetic field components in original and modified magnetic systems. Axial position measured from the backplane.

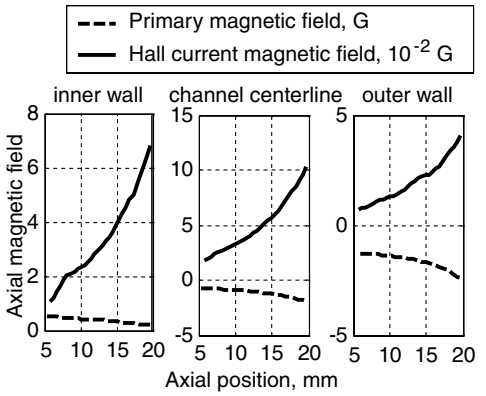

Fig. 4 Axial magnetic field component distribution of the primary magnetic field and the Hall current self-field in the region close to the backplane. Axial position measured from the backplane.

where

$$Z(z) = \frac{1}{\left[\frac{\sinh[a(z-c)]}{\sinh(aq)}\right]^2 + 1} \tag{1}$$

Here $R(r)$ is a Gaussian distribution and I_H is the normalization coefficient. Function $Z(z)$ includes three parameters: a, c, and q. Parameter a determines the slope steepness, c determines the median of the distribution, and q determines the width of the distribution. This function was chosen based on the following considerations: first, the experimental data [5,6,11] show that the Hall current distribution has a single maximum, and second, the results of calculations of plasma parameters distributions in [4] show that the axial distribution may be close to bell shaped but broader. This distribution allows obtaining both Gauss-like bell-shaped distributions as well as wider distributions.

In the calculations, a Hall current density distribution with a profile close to the experimentally measured [5,6] and a value of 10*A* was used. The comparison of the primary magnetic field distribution with the distribution of the self-field generated by the Hall current in the region close to the backplane (behind the anode) where the magnetic sensors could be placed is presented in Fig. 4. To plot the distributions on the same scale, the Hall current field was multiplied by a factor of 100. The magnitude of the Hall current self-field is significant enough (several percent of the primary field) to be measured by the existing magnetic sensors.

The calculations showed that the magnetic measurements in that area do not provide sufficient data for the determination of the Hall current distribution. Consequently, the magnetic screen should be modified. Fig. 5 shows the radial and axial magnetic field components' distribution in the modified part of the magnetic system where the magnetic sensors could be placed.

As can be seen, the ratio of the self-magnetic field to the primary field is much higher and even more so in the region where the axial component of the primary magnetic field is close to zero. This confirms the possibility of measuring the self-magnetic field in this region. The data provided by the sensors in this region, together with the data from the sensors located near the backplane, are sufficient for the Hall current determination. The schematic of magnetic sensor placement inside the Hall thruster is presented in Fig. 6.

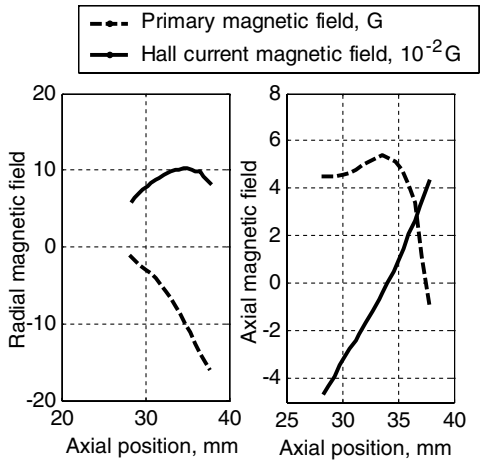

Fig. 5 Comparison of the primary magnetic field and the Hall current magnetic field in the region where the sensors may be placed. Axial position measured from the backplane.

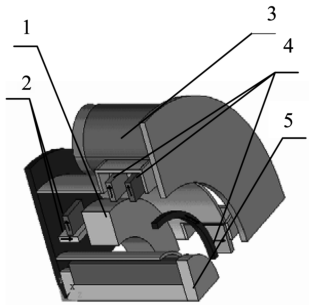

Fig. 6 Magnetic sensors placement inside Hall thruster. 1) Anode; 2) magnetic sensors behind the anode (arrows display the direction of the magnetic field component measured by the sensors); 3) modified part of outer magnetic screen; 4) magnetic sensors in the modified part of magnetic screen (arrows display the direction of the magnetic field component measured by the sensors); 5) current-carrying loop used for calibration ("calibration loop").

III. Inverse Problem

The inverse problem is the determination of the current distribution from the measured magnetic field values. Because steady-state (time-averaged) current and magnetic field distributions are considered, the problem is a magnetostatic problem.

Solution of the inverse magnetostatic problems has been discussed in the context of diagnostics of superconducting magnets [13], biomagnetism [14], identification of the plasma magnetic contour in the thermonuclear fusion area [15], and determination of the ferromagnetic thin shell magnetization [16]. Different regularization methods were used in these works: truncated singular value decomposition [15], iterative regularization [13], and the Levenberg–Marquard algorithm with regularization term [17]. In [16], instead of regularization, the authors use the injection of the physical information to constrain the solution. In this work, a different method is presented based on Tikhonov regularization [18].

A. Inverse Problem Formulation

As mentioned previously, the axisymmetric distribution of azimuthal current density is parameterized using piece-wise constant

elements. The discretization of the problem leads to the following linear matrix equation for determination of the magnetic field distribution:

$$Aj_H = B \tag{2}$$

The inverse problem can be formulated as a linear least-squares problem:

$$\min \|Aj_H - B\|^2 \tag{3}$$

It is necessary to determine the current distribution (vector j_H), which minimizes the quadratic residue between the calculated magnetic field and the measured field. This is the linearized approximation of the inverse magnetostatic problem.

The inverse magnetostatic problems are a particular case of the Fredholm integral equations of the first kind. They typically do not have a continuous inverse and are therefore ill posed [18]. Problems of this type are essentially underdetermined. The standard methods of linear algebra, such as LU (decomposition of a square matrix into a product of a lower triangular matrix and an upper triangular matrix), Cholesky, or QR factorization decomposition of a matrix into an orthogonal and a triangular matrix, cannot be used in a straightforward manner for their solution. It is necessary to incorporate some a priori information about the solution to stabilize the problem. This is the purpose of regularization. The key idea of the regularization is to approximate the discontinuous operator by a continuous one.

For our specific numerical example, the condition numbers of kernel matrices A, corresponding to radial and axial magnetic field components in the entire longitudinal cross section of the acceleration channel, are 8.9759×10^{17} and 3.4274×10^{18}. Obviously, these matrices are extremely ill conditioned. The condition number of matrix A is the measure of the sensitivity of the Eq. (2) solution for j_H to perturbations of the right side B. If the condition number is near 1, the problem and the matrix A are said to be well conditioned. If the condition number is much greater than 1 then the problem is ill conditioned. In this case small perturbations of B cause large perturbations in the solution. Therefore, even if we know the magnetic field distribution along the entire acceleration channel the straightforward solution of the inverse problem is impossible. The condition number of the matrix A corresponding to the chosen sensors locations is 616, and so the problem under consideration is also ill conditioned. Because the number of equations (equal to the number of sensors) is less than the number of unknown values (equal to the number of current elements), the problem is also rank deficient.

B. Regularization

There are different regularization techniques to overcome the difficulties of solving discrete ill-posed problems [18]. The most common form of regularization is Tikhonov regularization. In Tikhonov's method, the ill conditioning is circumvented by introducing a stabilizing term, which gives a new problem with a well-conditioned coefficient matrix. The truncated singular value decomposition (TSVD) method is based on replacing the small nonzero singular values from the decomposition of the operator by exact zeros, giving the approximate well-conditioned operator. In iterative regularization, the minimization problem [Eq. (3)] is solved using a conjugate gradient method generating a family of continuous operators with the iteration number as a regularization parameter. Maximum entropy regularization, which is used in image restoration and related applications, uses the solution entropy as a side constraint.

Different regularization methods were tested; the best results were obtained using the method based on Tikhonov regularization. The idea of the Tikhonov's method is to use a priori assumptions about the size and the smoothness of the desired solution. The general form of the Tikhonov's method for Eq. (3) takes the form

$$\min\lfloor \|Aj_H - B\|^2 + \lambda^2 \|Lj_H\|^2 \rfloor \tag{4}$$

where λ is the regularization parameter that controls the weight of the regularization term $\|Lj_H\|^2$ relative to the residual term $\|Aj_H - B\|^2$, and L is the regularization matrix, also called discrete smoothing form, which is a matrix that defines the norm of the solution through which the size is measured. Typically, L is the identity matrix, a diagonal weighting matrix, or a discrete approximation of a derivative operator. The choice of the regularization term depends on the a priori properties of the solution; that is, the additional information that is enforced on the regularization solution.

Different forms of the matrix L were tested, including the identity matrix corresponding to minimum-norm solution and different forms of two-dimensional derivative operators corresponding to the continuous and smooth solutions.

From physical considerations, the current distribution should be smooth, and the following regularization term was chosen:

$$\|L_{rr} j_H\|^2 + 2\|L_{rz} j_H\|^2 + \|L_{zz} j_H\|^2 \tag{5}$$

where

$$L_{rr} = \frac{\partial^2}{\partial r^2}, \qquad L_{rz} = \frac{\partial^2}{\partial r \partial z}$$

and

$$L_{rr} = \frac{\partial^2}{\partial z^2}$$

Additional constraints were added to the solution based on the physical features of the Hall current. The constraints used were as follows:

1) Nonnegativity constraint: The physical meaning of this constraint is that the azimuthal current in the entire acceleration channel flows in the same azimuthal direction. The solution obtained without this constraint includes some elements with negative currents. An example of such solution is presented.

2) Zero boundary condition: The Hall current density on the boundaries of the current distribution region is assumed to be zero. The boundaries are acceleration channel walls in radial direction, anode plane, and some plane normal to the thruster axis downstream of the thruster exit plane in the axial direction.

The second constraint is added to suppress the artifact secondary peaks that appear on the boundary of the solution region when measurement data are inexact.

The density of the Hall current is equal to

$$j_H = -en \frac{\mathbf{E} \times \mathbf{B}}{B^2} = -en \frac{E_z B_r - E_r B_z}{B^2} \tag{6a}$$

The main contribution to the thrust is produced in the exit and central regions of the acceleration channel. In these regions, the axial magnetic field is low in comparison with the radial magnetic field. The radial electric field, in turn, is low in comparison with the axial electric field. As a consequence, the product of the radial electric field by the axial magnetic field is much smaller than the product of the axial electric field by the radial magnetic field. Therefore, at least as a first approximation, it can be neglected compared with the contribution of the axial magnetic field to the Hall current:

$$j_H = -ne \frac{E_z}{B_r} \tag{6b}$$

The Hall current on the walls is equal to zero because the walls are made of insulator materials, and the number density of the free electrons on them is zero.

We will now show that the Hall current density on the anode is negligible and can be assumed to be zero.

When taking into account collisional processes in a conducting medium, the Hall current density is equal to

$$j_H = -\frac{\sigma_0 \omega_e \tau_e}{1 + \omega_e^2 \tau_e^2} E_z = -\frac{ne^2}{m} \tau_e \frac{\omega_e \tau_e}{1 + \omega_e^2 \tau_e^2} E_z \tag{6c}$$

where m is the mass of the electron, τ_e is the time between electron collisions with heavy particles or walls,

$$\sigma_0 = \frac{ne^2}{m}\tau_e$$

is the electrical conductivity,

$$\omega_e = \frac{e|B_r|}{m}$$

is the electron cyclotron frequency, and $\omega_e\tau_e$ is the Hall parameter. Because in the Hall thruster plasma, $\omega_e\tau_e \gg 1$, we obtain Eq. (6b).

In the anode material, the density of heavy particles is by a factor of $\sim 10^9$ higher than in the plasma. Consequently, τ_e is by many orders less than in the plasma, and $\omega_e\tau_e \ll 1$. Therefore, according to Eq. (6c), in the anode

$$|j_{\text{an}H}| \ll |i_{\text{an}z}| = \sigma_{0\text{an}} E_{\text{an}z} \tag{6d}$$

where the index "an" means that the quantities correspond to the anode. The density of the longitudinal current in the anode, $j_{\text{an}z}$, is of the same order of magnitude as the density of the discharge current in the plasma j_d. Therefore, from Eq. (6d) and taking into account the fact that in the Hall thruster plasma the density of the Hall current is greater than j_d, it follows that the density of the Hall current in the anode is much smaller than in the acceleration channel plasma and can be considered as a negligibly small quantity, as previously stated.

Outside the acceleration channel, the electric field drops to zero, and the Hall current also drops to zero at a certain distance from the thruster exit plane.

C. Optimization Method

A constrained minimization algorithm implemented was used to solve Eq. (4). It is a sequential quadratic programming algorithm, which consists of three main implementation stages: 1) updating the Lagrangian function Hessian, 2) quadratic programming problem solution, and 3) line search.

The solution procedure is as follows: the simulated measurements are obtained using the linear system, and then the inverse problem is solved using the constrained optimization method. The optimization procedure starts with values of current in all elements set to zero. Measurement errors were simulated by adding a Gaussian random noise to the exact data.

The regularized problem includes three derivatives and additional constraints, which makes it different from the traditional Tikhonov regularization. For that reason, it proved impossible to use the usual methods such as L-curve for the regularization parameter choice. The parameter was chosen manually by the method described here.

IV. Numerical Results

For the numerical solution of the inverse problem, a MATLAB program has been developed. Using the methods described previously, the inverse problem is solved using either exact or perturbed values of the magnetic field.

Let us consider the current distribution presented in Fig. 7. The peak of the distribution is situated several millimeters upstream of the exit plane close to the outer channel wall. This distribution is similar to the experimentally measured distribution of the Hall current density [5,6]. The peak of the current density is located several millimeters upstream of the exit plane, with some portion of the current flowing outside the acceleration channel. The simulated magnetic field values of the magnetic sensors located outside the acceleration channel are in the range of 1–10 mG. The maximum self-magnetic field values in the acceleration channel were in the range of several Gauss, which is the same order of magnitude as the results of Haas and Gallimore [5,6].

A. Regularization

The various steps of the numerical solution process are now presented. Solving the minimization problem without the constraints and regularization term gives the results shown in Fig. 8. Obviously, the solution is far from the exact distribution, and it has no physical sense because the current density in some locations is negative (i.e., the currents in different elements flow in different azimuthal directions). Adding the nonnegativity constraint, we obtain the solution shown in Fig. 9. This solution is also very far from the current distribution shown in Fig. 7. Adding the regularization term described previously to obtain the smooth distribution will give the result presented in Fig. 10. This result is still far from the original distribution. However, now this distribution is continuous and smooth. This is the result of the regularization term addition. Adding the zero constraint at the borders of the solution domain, we obtain the solution shown in Fig. 11. This solution is sufficiently close to the exact current distribution. The position of its peak coincides with the corresponding position of the exact distribution; radial and axial widths of distribution are very close to those of the original distribution. The total current corresponding to this distribution is 10.4*A*, which is close to the original value of 10*A*.

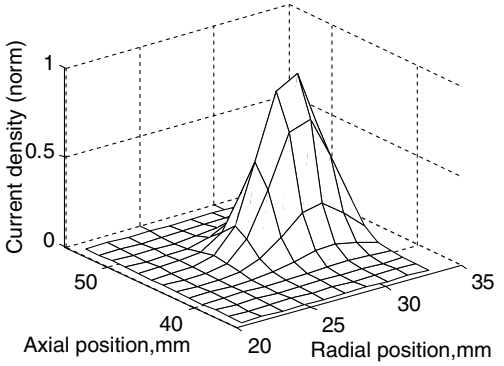

Fig. 7 The Hall current distribution used for simulated measurements and inverse problem solution. Position of the maximum: $z = 46$ mm, $r = 30$ mm; total Hall current is 10A.

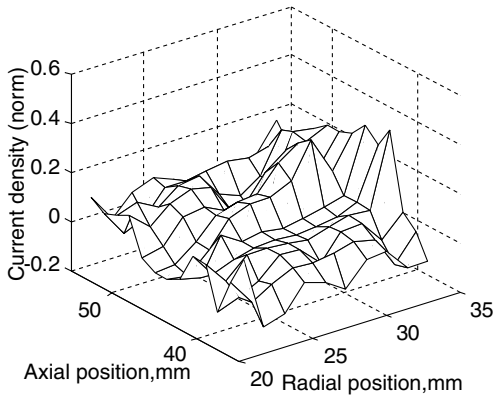

Fig. 8 Solution of the inverse problem without regularization and constraints.

The radially averaged axial profiles, as well as the axially averaged radial profiles corresponding to the original distribution and to the distribution calculated from simulated measurements, are presented in Fig. 12. It should be emphasized that our objective is to obtain as much information as possible about the Hall current distribution, but it is impossible to obtain the exact distribution from the regularized solution. Besides, accuracy is limited because only a limited number of sensors placed in specific locations can be used. In Fig. 12, it is clearly seen that the obtained solution is sufficiently close to the exact one.

B. Choice of Regularization Parameter

An important stage of the solution is the choice of the regularization parameter. This parameter accounts for the degree of smoothness of the regularized solution. The most commonly used method for the regularization parameter choice is the L-curve method [18]. The L

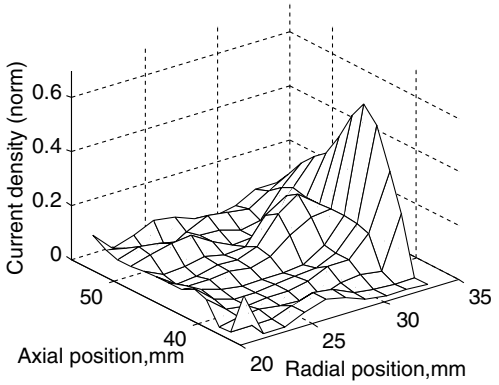

Fig. 9 Solution of the inverse problem with nonnegativity constraint.

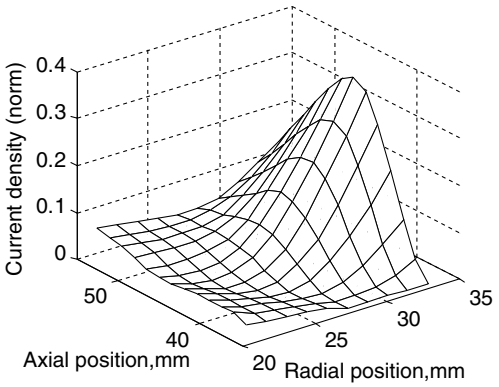

Fig. 10 Solution of the inverse problem with a regularization term.

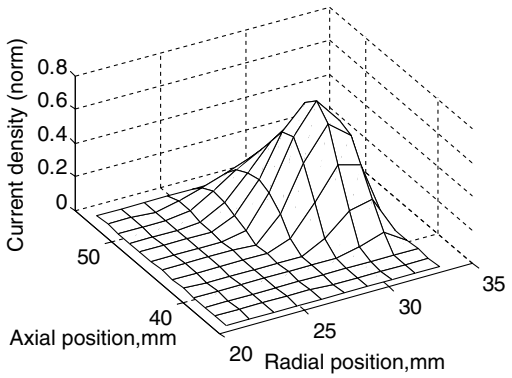

Fig. 11 The regularized solution with unperturbed measurements.

curve is the parametric plot of the discrete smoothing norm, that is, the norm of the regularization term $\|Lj_H\|^2$ versus the corresponding residual norm $\|A \times j_H - B_m\|^2$. For many discrete ill-posed problems, this curve plotted in log–log scale has a characteristic L shape with a distinct corner separating its horizontal and vertical parts. According to the L-curve criterion, the value of the regularization parameter corresponding to the L-curve corner is the optimal value. In our case, the curve does not have the L shape, and the optimal value of the regularization parameter does not correspond to its distinct corner. The reason is that in this case the residual norm and the smoothing norm are not monotonic functions of the regularization parameter. Another popular method for choosing the regularization parameter is the discrepancy principle. It requires the knowledge or a good estimate of the error norm. It is not possible to use it because the error norm is not known. The generalized cross validation (GCV) method also cannot be used in this case.

When it is not possible to use the parameter-choice methods, the regularization parameter may be also chosen by visual inspection of the solution [19,20]. Because the parameter varies in the range

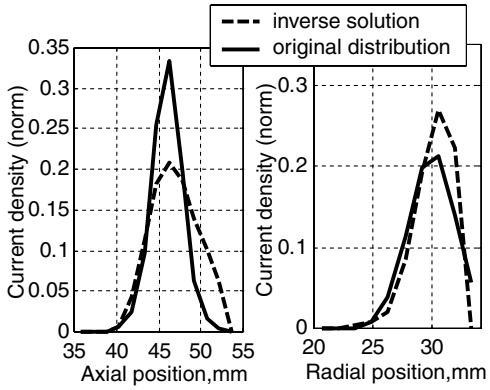

Fig. 12 Axial and radial profiles of original and calculated distributions.

10^{-3}–10^{0}, which is not very wide, this procedure is not very time consuming.

The parameter-choice procedure is demonstrated in Fig. 13. The set of solutions is obtained for different regularization parameter values, and the minimal value corresponding to a relatively smooth solution with a single peak is chosen. In the solution presented here, 10 parameter values in the range 10^{-3}–10^{0}, uniformly spaced on the logarithmic scale, were used. Several solutions are presented in Fig. 13. Corresponding regularization parameter values and total current values are presented in the plots.

The solutions with a low regularization parameter value are not smooth; they have several sharp peaks and obviously may not be chosen. As the regularization parameter value increases, the solutions become smoother, and the last two solutions are sufficiently smooth and have one distinct peak. The solution corresponding to the regularization parameter value 0.0215 is finally chosen in this case. The comparison of the solution with the original distribution was presented in Fig. 12.

C. Choice of Optimal Number of Sensors

To determine the optimal number of magnetic sensors, at first the maximum sensors number was assessed (i.e., all possible probe placements were determined). The initial assessment showed that the sensors may be placed in two regions inside thruster: in the box fitted to the magnetic screen that was mentioned previously and close to the thruster backplane, where the ratio of the Hall current self-field and primary magnetic field is also sufficiently high. Ten possible sensor locations were chosen as follows: six behind the anode, equally spaced in the radial direction, and four in the modified part of the outer magnetic screen. In every one of these points, both axial and radial magnetic field components can be measured, giving the overall number of 20 sensors.

Then the analysis was performed to choose the optimal number of magnetic sensors. As described previously, each sensor corresponds to the row of the matrix A of Eq. (2), which was also described on Fig. 2. Therefore, the choice of the optimal set of sensors corresponds to the choice of the optimal set of the rows of matrix A from the given 20 rows. The following method was used: for the matrix with N rows, we may form N matrices with $N-1$ rows, excluding consecutive row numbers $1, 2, \ldots, N$ from the initial matrix. From these matrices, the one with the lowest condition number is chosen (the condition number of a matrix measures the sensitivity of the solution of a system of linear equations to errors in the data). Applying this method for N (corresponding to the number of sensors), consecutively changing from 20 to 3, we obtain 18 matrices corresponding to 18 sets with different numbers of sensors.

The inverse solutions corresponding to different sets of sensors are shown in Fig. 14. The arrow indicates the inverse solution variation with the decrease of the number of sensors. As expected, the solution accuracy deteriorates as the number of sensors decreases.

To study the tradeoff between the solution accuracy and the number of sensors, two figures of merit were used. The first is the relative error:

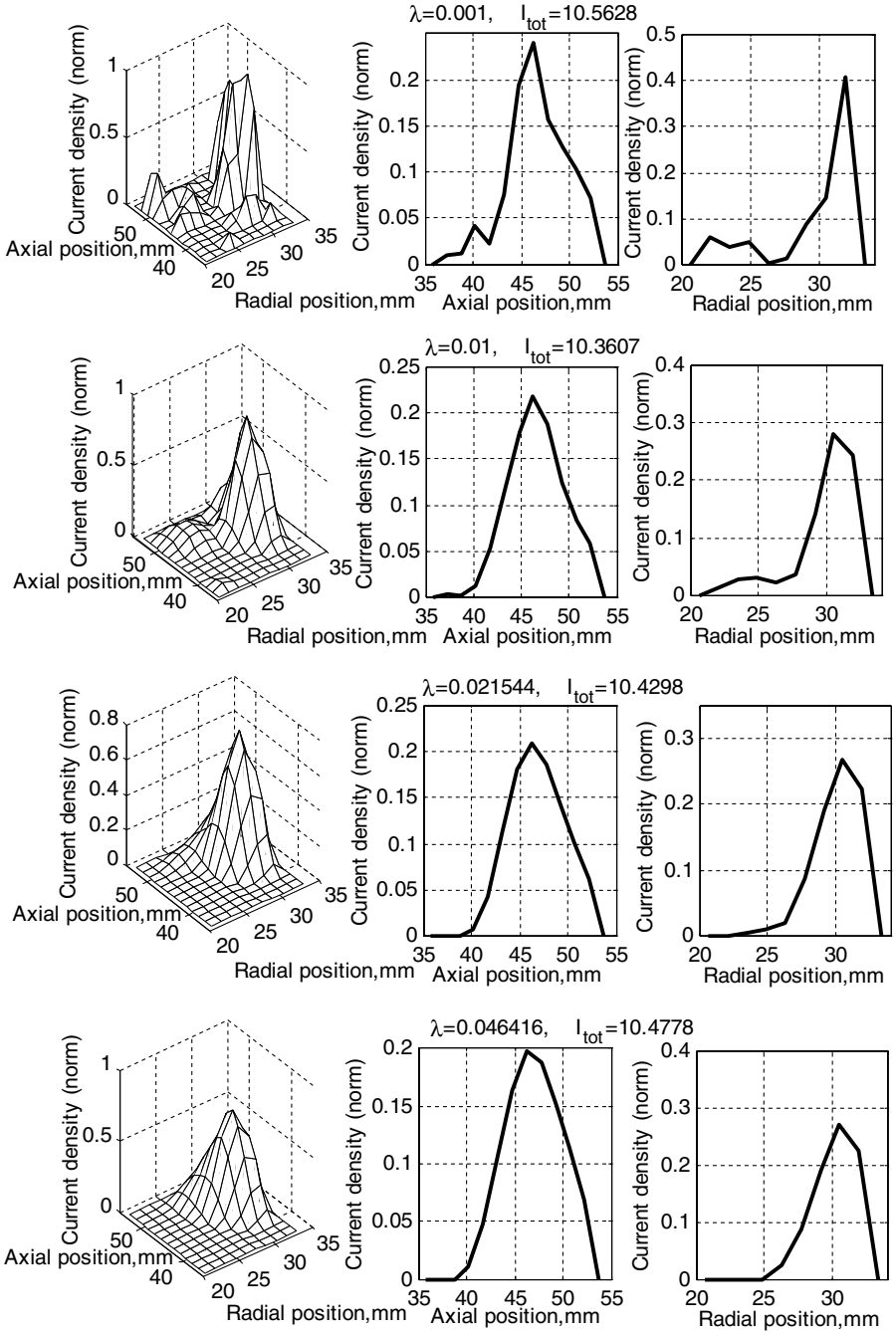

Fig. 13 Solutions corresponding to different values of the regularization parameter.

$$D = \sum_{i,j} \frac{\|j_{ij}^{\text{inverse}} - j_{ij}^{\text{exact}}\|_2}{\|j_{ij}^{\text{exact}}\|_2} \tag{7}$$

The second is the thrust calculated using the following equation:

$$T = \int_V |j_H B_r| \, \mathrm{d}V = \sum_{ij} j_{ij} B_{ij_r} \Delta V \tag{8}$$

where B_r, B_{ij} is the radial component of the primary magnetic field generated by the thruster's magnetic system, calculated using FEM.

The results presented here were obtained using the noise-free values of the simulated magnetic field measurements. Real measurements are always contaminated with noise. To choose the optimal number of sensors, it is also necessary to examine the inverse problem solutions with simulated noise added to the magnetic field values.

It is also necessary to determine the dependences of the solution accuracy on the noise level to estimate the accuracy of the Hall current determined from the experimental data. The measurement error can be estimated by statistical techniques, and using the results presented here, we can estimate the accuracy of the inverse problem solution. These data are also required to determine the limitation on the level of current oscillations in magnetic coils. These oscillations should be limited to increase the measurements' accuracy.

Noise was added to the simulated measurements using the following expression:

$$B_i^* = B_i(1 + d\xi) \tag{9}$$

where B_i and B_i^* are exact and "measured" magnetic field values for the ith sensor, and ξ is a normally distributed random number with mean 0 and standard deviation 1. The noise level d varied in the range of 0.025–0.1, corresponding to the error's standard deviation in the range of 2.5–10%.

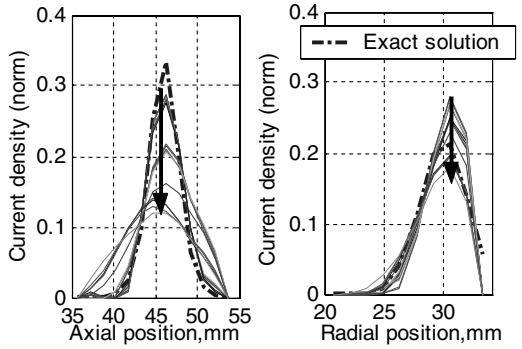

Fig. 14 Inverse problem solutions for different number of sensors.

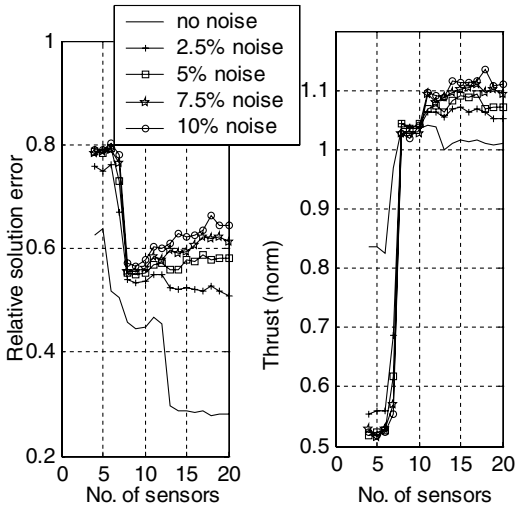

Fig. 15 Average relative solution error and thrust values vs the number of sensors at different noise levels.

For every sensors set and noise level, 400 simulated measurements, corresponding to the same exact magnetic field values, were generated. The inverse problem was solved using that value; relative error and thrust values corresponding to a particular noise level and sensors set were averaged. The dependences of these values on the number of sensors for different noise levels (including 0% level, no noise) are presented in Fig. 15. Thrust values were normalized to the exact value.

Without noise, the relative solution error is almost constant for 13 or more sensors, jumps when the number drops below 13, and grows when the number reduces below 8. Thrust is very close to the exact value for 13 and more sensors and varies significantly for seven sensors and less. Up to this point, it seems reasonable to choose the set of 13 sensors. However, the situation is different when noise is added. As seen from Fig. 15, for a large sensor number, the average solution error and the average error in calculated thrust grow stronger with measurement noise growth. It happens because the matrices corresponding to the large number of sensors are highly ill conditioned and therefore very sensitive to noise. When the noise level is 10%, the average error is less for 10 sensors than for 20.

We see that it can be unreasonable to choose too large a sensor set because increasing the number of sensors to more than 13 gives little or no improvement in the case of exact measurements and may deteriorate the accuracy if large errors are present, but it also should not be too small. From Fig. 15, one can see that the sensor sets including fewer than eight sensors do not contain the information necessary for a reasonably accurate solution leading to high errors. At least one sensor placed in the modified part of the magnetic screen is necessary, which is not the case for sets with seven and fewer sensors. Therefore, we choose the set including 10 sensors. This set includes one sensor placed in the modified part of the magnetic screen and nine sensors near the thruster backplane. The solution corresponding to noise-free measurement obtained using this set is presented in Fig. 12.

D. Numerical Example Based on Published Experimental Data

To evaluate how the proposed method will perform for other Hall thruster models, the data of Haas and Gallimore [5,6] on azimuthal current distribution in a Hall thruster were used. In this numerical example, the computations for the P5 Hall thruster were performed using the Hall current distributions published in [5,6]. The magnetic system dimensions of the P5 thruster were taken from [21]. Primary magnetic field distributions for the P5 thruster were taken from [7], because only inner wall, centerline, and outer wall distributions were given; tensor spline was used to obtain the distribution in the entire acceleration channel. In the simulations, it is assumed that the magnetic sensors are placed into the P5 thruster. The locations of the sensors are analogous to the locations determined here: one sensor in the region close to the exit plane and nine sensors near the thruster backplane. The algorithm of the direct problem solution described in Sec. II.A is used to calculate the kernel matrix for this thruster. Because the magnetic screens of the P5 thruster are axially symmetric, the 2-D axisymmetric calculations of magnetic field using the finite element method magnetics solver were performed.

To simulate the magnetic field measurements for sensors located outside the acceleration chamber, the Hall current distributions were approximated by fitting Eq. (1) to experimental data from [5,6]. Then, using the kernel matrix, simulated magnetic field measurements were calculated, and the inverse problem was solved.

The comparison of the Hall current distributions approximated to experimental data from [5,6], and the solutions of the inverse problem are presented in Figs. 16 and 17.

Thrust values were calculated for the approximated distributions and the inverse problem solutions using Eq. (8). For the 1.6 kW mode, the thrust value corresponding to the approximated distribution is 103.1 mN, and the value corresponding to the inverse problem solution is 101.1 mN. The value calculated from the experimental data [5,6] is 93 mN, and the directly measured value is 95 mN. For the 3 kW mode, thrust values corresponding to the approximated distribution and to the inverse problem solution are 181.9 and 179.3 mN, respectively; calculated and measured values from 5 and 6 are −168 and 175 mN. The discrepancy between the thrust values in [5,6] and the thrust calculated using the approximated distribution is due to inaccuracy in the approximation of the current

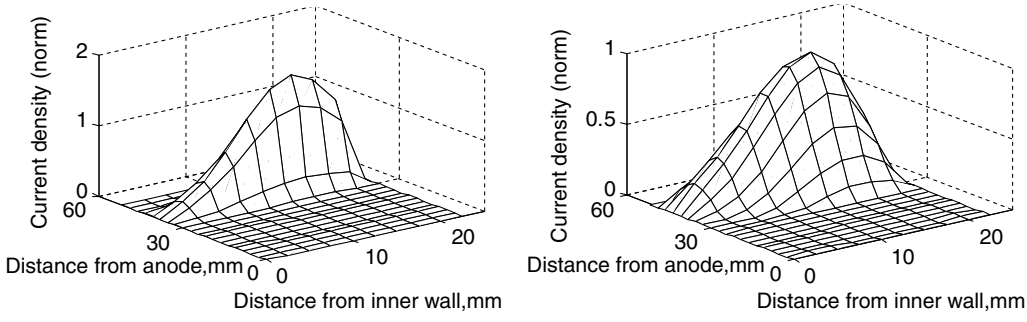

Fig. 16 Hall current distribution. 1.6 kW mode. Left) experimental data fit; right) inverse problem solution.

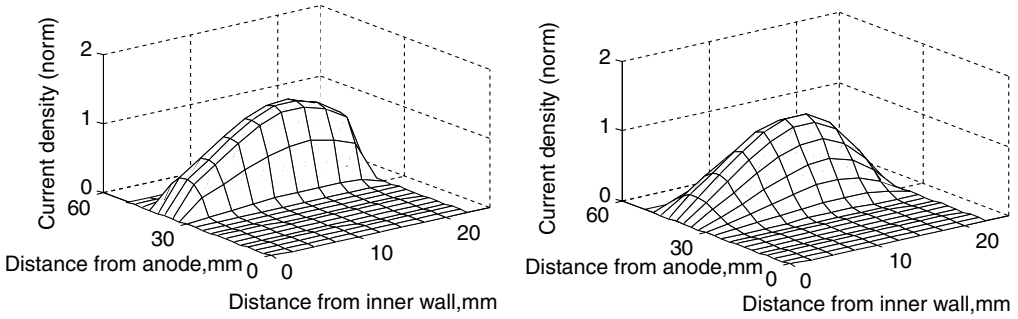

Fig. 17 Hall current distribution, 3 kW mode. Left) fitted to experimental data; right) inverse problem solution.

distribution and interpolation of the primary magnetic field. Nevertheless, this discrepancy makes less than 10% of the exact value, and this example demonstrated that the proposed technique can be used for thrust estimation after adequate calibration.

V. Conclusions

1) A new method for determination of the Hall current structure inside the Hall thruster acceleration channel is developed. It is shown that the Hall current structure can be determined using noncontact steady-state measurements of the magnetic field. The method is based on two-dimensional constrained regularization.

2) The solution algorithm was tested using both noiseless and noisy simulated magnetic measurements. The tradeoff between the sensors number and solution accuracy was studied and the optimal number and positions of sensors were determined.

3) The method was tested using published data on Hall current distributions measured in experiments with the P5 Hall thruster.

4) The implementation of the proposed method requires minor modification of the thruster. The hardware necessary to carry out the measurements is quite simple. The proposed method is to be validated in experiments.

References

[1] Manzella, D., Jankovsky, R., Elliott, F., Mikellides, I., Jongeward, G., and Allen, D., "Hall Thruster Plume Measurements On-Board the Russian Express Satellites," Electric Rocket Propulsion Society Paper 2001-044, Oct. 2001.

[2] Arhipov, B., Krochak, L., Maslennikov, N., and Scortecci, F., "Investigation of the Operating Characteristics of a High-Power Hall Effect Thruster," *Journal of Propulsion and Power*, Vol. 16, No. 5, 2000, pp. 910–915.

[3] Kapulkin, A., Kogan, A., and Guelman, M., "Noncontact Emergency Diagnostics of Stationary Plasma Thruster in Flight," *Acta Astronautica*, Vol. 55, No. 2, July 2004, pp. 109–119. doi:10.1016/j.actaastro.2004.04.001

[4] Rubin, B., Guelman, M., and Kapulkin, A., "Principles of Hall Thruster Onboard Malfunction Diagnostics Based on Magnetic Field Measurements of Plasma Currents," *Proceedings of the Fourth International Spacecraft Propulsion Conference*, SP-555, ESA, June 2004, [CD–ROM].

[5] Haas, J. M., and Gallimore, A. D., "Considerations on the Role of the Hall Current in a Laboratory-Model Thruster," AIAA Paper 2001-3507, July 2001.

[6] Haas, J. M., and Gallimore, A. D., "Considerations on the Role of the Hall Current in a Laboratory-Model Thruster," *IEEE Transactions on Plasma Science*, Vol. 30, No. 2, 2002, pp. 687–697. doi:10.1109/TPS.2002.1024271

[7] Peterson, P. Y., Gallimore, A. D., and Haas, J. M., "An Experimental Investigation of the Internal Magnetic Field Topography of an Operating Hall Thruster," *Physics of Plasmas*, Vol. 9, No. 10, 2002, pp. 4354–4362. doi:10.1063/1.1507771

[8] Demyanenko, V. N., Zubkov, I. P., Lebedev, S. V., and Morozov, A. A., "Induction Method for Measuring the Azimuthal Drift Current in a Hall-Current Accelerator," *Soviet Physics, Technical Physics*, Vol. 23, No. 3, March 1978, pp. 376, 377.

[9] Bugrova, A. I., Versotskii, V. S., and Kharchevnikov, V. K., "Determination of the Radial Center of Gravity of an Azimuthal Drift Current in Accelerators with Closed Electron Drift," *Soviet Physics, Technical Physics*, Vol. 25, No. 10, Oct. 1980, pp. 1307–1309.

[10] Prioul, M., Bouchoule, A., Roche, S., Magne, L., Pagnon, D., Touzeau, M., and Lasgorceix, P., "Insights of Hall Thrusters Through Fast Current Interruptions and Discharge Transients," Electric Rocket Propulsion Society Paper 01-059, Oct. 2001.

[11] Thomas, C. A., Gascon, N., and Cappelli, M. A., "Non-Intrusive Characterization of the Hall Thruster Azimuthal Drift Current," AIAA Paper 2004-3776, July 2004.

[12] Kim, V., "Main Physical Features and Processes Determining the Performance of Stationary Plasma Thrusters," *Journal of Propulsion and Power*, Vol. 14, No. 5, 1998, pp. 736–743.

[13] Begot, S., Voisin, E., Hiebel, P., Kauffmann, J. M., and Artioukhine, E. A., "Resolution of Linear Magnetostatic Inverse Problem Using Iterative Regularization," *The European Physical Journal. Applied Physics*, Vol. 12, No. 2, Nov. 2000, pp. 123–131. doi:10.1051/epjap:2000179

[14] Nenonen, J. T., "Solving the Inverse Problem in Magnetocardiography," *IEEE Engineering in Medicine and Biology Magazine*, Vol. 13, Aug./Sept. 1994, pp. 487–496. doi:10.1109/51.310989

[15] Bettini, P., Bellina, F., Formisano, A., Martone, R., Stella, A., and Trevisan, F., "Identification of the Plasma Magnetic Contour from External Magnetic Measurements by Means of Equivalent Currents," *The European Physical Journal. Applied Physics*, Vol. 13, No. 1, Jan. 2001, pp. 51–58. doi:10.1051/epjap:2001101

[16] Chadebec, O., Coulomb, J.-L., Bongiraud, J.-P., Cauffet, G., and Le Thiec, P., "Recent Improvements for Solving Inverse Magnetostatic Problem Applied to Thin Shells," *IEEE Transactions on Magnetics*, Vol. 38, No. 2, March 2002, pp. 1005–1008. doi:10.1109/20.996258

[17] Russenschuk, S., Calmon, F., Lewin, M., Ramberger, S., Rodriguez-Mateos, F., Tortschanoff, T., Verweij, A., and Wolf, R., "Integrated Design of Superconducting Accelerator Magnets. A Case Study of the Main Quadrupole," *The European Physical Journal. Applied Physics*, Vol. 1, No. 1, Jan. 1998, pp. 93–102. doi:10.1051/epjap:1998122

[18] Hansen, P. C., *Rank-Deficient and Discrete Ill-Posed Problems: Numerical Aspects of Linear Inversion*, SIAM Monographs on Mathematical Modeling and Computation 4, SIAM, Philadelphia, 1997, pp. 4–13, 99–106, 187–192.

[19] Merwa, R., Hollaus, K., Brunner, P., and Scharfetter, K., "Solution of the Inverse Problem of Magnetic Induction Tomography (MIT)," *Physiological Measurement*, Vol. 26, March 2005, pp. S241–S250. doi:10.1088/0967-3334/26/2/023

[20] Casanova, R., Silva, A., and Borges, A. R., "Magnetic Induction Tomography Imaging Using Tikhonov Regularization," *Workshop on Inverse Obstacle Problems*, International Association for Mathematics and Computers in Simulation, Lisbon, 2002, http://www.math.ist.utl.pt/wiop/Wiop-2002-pg.html#poster.

[21] Hofer, R. R., Haas, J. M., Peterson, P. Y., Martinez, R. A., and Gallimore, A. D., "Optimization of Hall Thruster Magnetic Field Topography," International Conference on Plasma Science, Paper 00-5P02, June 2000.

A. Gallimore
Associate Editor